



Stem cell migration and mechanotransduction on linear stiffness gradient hydrogels

William J. Hadden^{a,1}, Jennifer L. Young^{b,c,1}, Andrew W. Holle^{b,c,1}, Meg L. McFetridge^d, Du Yong Kim^e, Philip Wijesinghe^{f,g}, Hermes Taylor-Weiner^h, Jessica H. Wen^h, Andrew R. Lee^h, Karen Bieback^{i,j}, Ba-Ngu Vo^e, David D. Sampson^{f,k}, Brendan F. Kennedy^{g,l}, Joachim P. Spatz^{b,c}, Adam J. Engler^{h,m}, and Yu Suk Choi^{a,d,2}

^aKolling Institute for Medical Research, University of Sydney, St Leonards NSW 2065, Australia; ^bDepartment of Cellular Biophysics, Max Planck Institute for Medical Research, 69120 Heidelberg, Germany; ^cDepartment of Biophysical Chemistry, University of Heidelberg, D-69120 Heidelberg, Germany; ^dSchool of Human Sciences, University of Western Australia, Perth WA 6009, Australia; ^eDepartment of Electrical and Computer Engineering, Curtin University, Perth WA 6102, Australia; ^fOptical+Biomedical Engineering Laboratory, School of Electrical, Electronic and Computer Engineering, University of Western Australia, Perth WA 6009, Australia; ^gBioimaging Research and Innovation for Translational Engineering Laboratory, Harry Perkins Institute of Medical Research, Queen Elizabeth II Medical Centre, Perth WA 6009, Australia; ^hDepartment of Bioengineering, University of California, San Diego, CA 92093; ⁱInstitute of Transfusion Medicine and Immunology, Medical Faculty Mannheim, Heidelberg University, D-68167 Mannheim, Germany; ^jGerman Red Cross Blood Service Baden-Württemberg – Hessen, D-68167 Mannheim, Germany; ^kCentre for Microscopy, Characterisation & Analysis, University of Western Australia, Perth WA 6009, Australia; ^lSchool of Electrical, Electronic and Computer Engineering, University of Western Australia, Perth WA 6009, Australia; and ^mSanford Consortium for Regenerative Medicine, San Diego, CA 92037

Edited by David A. Weitz, Harvard University, Cambridge, MA, and approved April 24, 2017 (received for review November 4, 2016)

The spatial presentation of mechanical information is a key parameter for cell behavior. We have developed a method of polymerization control in which the differential diffusion distance of unreacted cross-linker and monomer into a prepolymerized hydrogel sink results in a tunable stiffness gradient at the cell-matrix interface. This simple, low-cost, robust method was used to produce polyacrylamide hydrogels with stiffness gradients of 0.5, 1.7, 2.9, 4.5, 6.8, and 8.2 kPa/mm, spanning the *in vivo* physiological and pathological mechanical landscape. Importantly, three of these gradients were found to be nondurotactic for human adipose-derived stem cells (hASCs), allowing the presentation of a continuous range of stiffnesses in a single well without the confounding effect of differential cell migration. Using these nondurotactic gradient gels, stiffness-dependent hASC morphology, migration, and differentiation were studied. Finally, the mechanosensitive proteins YAP, Lamin A/C, Lamin B, MRTF-A, and MRTF-B were analyzed on these gradients, providing higher-resolution data on stiffness-dependent expression and localization.

mechanobiology | stem cell migration | stem cell differentiation | extracellular matrix | stiffness

Stem cells receive a myriad of chemical and mechanical cues from their environment and must integrate those signals to commit to a specific lineage. Although the ability of chemical signals (soluble and/or substrate-immobilized) to dictate stem cell behavior in the microenvironment has been appreciated for decades, only recently has significant research focus shed light on the mechanical forces that shape organismal development and direct disease response (1–3). Chemical gradients impacting stem cell migration, proliferation, and differentiation are well-described, and methods permitting their wide-scale use now allow efficient investigation of the effects they elicit (4–6).

Mechanotransduction is arguably more intuitive, as the functional boundaries at multiple length scales in living systems attest. Physiological interfaces, such as those at neuromuscular junctions, and pathological boundaries, e.g., infarcted fibrous heart tissue adjacent to healthy myocardium, are prevalent *in vivo* and imply that mechanical cues not only help guide differentiation but play critical regulatory roles in disease response. Recent studies have identified substrate stiffness as a significant factor in cell spreading (7, 8), migration (9), proliferation (10), and differentiation (11, 12) using both adipose-derived (13) and bone marrow-derived stem cells (14). When mimicking the stiffness of neural (~1 kPa), muscle (~12 kPa), and bone (~30 kPa) tissues (15, 16), substrate stiffness can induce differentiation toward those specific tissue types. Furthermore, stem cells will migrate toward regions of higher stiffness in a process known as “durotaxis”

(17–19), whereas neurons have shown preference for softer regions (20, 21). Additionally, some cancer cell lines are inversely sensitive to substrate stiffness and thus show markedly different migration phenotypes (22–24). Given these complex and differential responses, it is apparent that any thorough *in vitro* investigation of stem cell behavior must consider both the absolute substrate stiffness value and the underlying stiffness gradient strength.

To create stiffness gradients *in vitro*, a multitude of diverse methods have been proposed, including repeated freeze-thaw methods with liquid nitrogen and cylindrical polyvinyl alcohol columns (25), heat gradients within polymerizing polydimethylsiloxane (PDMS) (10), polyelectrolyte monolayers with a patterned cross-linker (26), inclusion of rigid particles in a soft hydrogel (27), and microfluidic mixing of different polyacrylamide (PA) solutions. However, all require significant technical background or equipment or are exceedingly expensive. Other less complex methods use photoinitiators and a patterned (28–30) or moving (31–33) photomask overlying a polymerization chamber to create stiffness gradients, although they are limited by the penetration depth of the light source, nonhomogeneous diffusion of photons, and residual toxicity of initiators left within the polymerized

Significance

Mechanobiology is receiving an increasing amount of focus, but the mechanics of cell-substrate behavior are often neglected in cell biology. As such, novel materials and systems that are simple to build and share in a nonengineering laboratory are sorely needed. We have fabricated gradient hydrogels with continuous linear gradients above and below the durotactic threshold, making it possible to pinpoint optimal stiffness values for a wide range of biological phenomena without the confounding effects of durotaxis. This system has the potential for wide adoption in the cell biology community because of its ease of fabrication, simple material ingredients, and wide gradient possibilities in a single well.

CELL BIOLOGY

Author contributions: J.L.Y., A.W.H., and Y.S.C. designed research; W.J.H., J.L.Y., A.W.H., M.L.M., P.W., H.T.-W., J.H.W., A.R.L., A.J.E., and Y.S.C. performed research; K.B., B.-N.V., D.D.S., B.F.K., J.P.S., A.J.E., and Y.S.C. contributed new reagents/analytic tools; W.J.H., J.L.Y., A.W.H., M.L.M., D.Y.K., P.W., H.T.-W., J.H.W., B.F.K., A.J.E., and Y.S.C. analyzed data; and W.J.H., J.L.Y., A.W.H., A.J.E., and Y.S.C. wrote the paper.

The authors declare no conflict of interest.

This article is a PNAS Direct Submission.

Freely available online through the PNAS open access option.

¹W.J.H., J.L.Y., and A.W.H. contributed equally to this work.

²To whom correspondence should be addressed. Email: yusuk.choi@uwa.edu.au.

This article contains supporting information online at www.pnas.org/lookup/suppl/doi:10.1073/pnas.1618239114/-DCSupplemental.

gel. Indeed, studies performed with gradient photomasks for UV photopolymerization have shown poor reproducibility and gradient linearity (19). Recent work has demonstrated the ability to build stiffness gradients in PA based on diffusion-driven gradients, although these methods require photolithography and microfluidics (34). Thus, although simple methods exist to produce chemical gradients (4–6), protocols to create simple (i.e., not requiring a clean room or photolithography facility) and highly reproducible [i.e., not relying on photopolymerization or PDMS interfaces] linear mechanical gradients spanning all biologically relevant ranges remain elusive (Table S1) (15, 35). Our aim is to develop a simple, nontoxic, cost-effective, and highly reproducible culture surface that puts stiffness gradient control into the hands of cell biology researchers who may not otherwise have access to more complex methods. To do so, we have investigated the stiffness-sensitive expression of the known mechano-regulator YAP (Yes-associated protein), the nuclear “mechanostat” Lamin A and its less stiffness-sensitive counterpart Lamin B, and the transcription factors MRTF-A and MRTF-B to a higher stiffness resolution than previously attained, revealing heretofore unobserved “transition zones” between basal and saturated levels of mechanosensitive proteins.

Results and Discussion

Stiffness Gradient Hydrogel Fabrication: A Two-Step Polymerization Process

Previous methods of reproducing *in vivo* stiffness gradients in culture systems are either complex (19, 30, 34, 36, 37) or lack the stiffness or gradient range (9, 30, 32) to interrogate the physiological mechanical landscape fully (Table S1). Therefore, we developed a method to fabricate planar PA hydrogels with linear stiffness gradients capable of spanning both biologically relevant ranges and disease conditions. Briefly, 24 × 20 × 1 mm glass molds were constructed from glass slides, coverslips, and cyanoacrylate. Aliquots (250 μL) consisting of a defined acrylamide monomer concentration (4, 6, 9, 12, or 15%) and 0.4% *N,N*-methylene-bis-acrylamide cross-linker (Fig. 1A, i) were poured into a dichlorodimethylsilane (DCDMS)-treated glass mold and covered with a 3-(trimethoxysilyl)-propyl methacrylate (3-TMPM)-treated glass coverslip so that the polymerization chamber assumed the shape of a right-angled ramp with a 3° angle in the vertical plane (Fig. 1A, ii). The functionalized coverslip reacts with the PA solution and subsequently serves as a support for manipulating the hydrogel. After polymerization and removal from the mold (Fig. 1A, iii and iv), a second 280-μL aliquot of acrylamide (6, 9, 12, 15, 16, or 20%) was poured into the mold and covered with the first PA gel (Fig. 1A, v) so that the coverslip edge overhangs (Fig. 1A, vi). After polymerization of the second component, the compound structure was removed from the mold (Fig. 1A, vii and viii), yielding a 24 × 20 × 1-mm PA hydrogel composed of two sequentially polymerized, inversely oriented, ramp-shaped components. Ultimately, this system requires only acrylamide/bis-acrylamide solution, DCDMS, 3-TMPM, glass slides and coverslips, and cyanoacrylate glue (as few as five common laboratory chemicals and supplies) for the fast formation of gradient hydrogels suitable for cell biology studies. Furthermore, because of the large, consistent surface area presented to the cells, this system can assay higher numbers of cells per gel than any other stiffness-gradient tool available (Table S1).

Topographical and Mechanical Characterization. Varying the concentration of acrylamide monomer can substantially alter the stiffness of a planar PA surface (38). We therefore postulated that an interface with a uniform slope between two sequentially polymerized components of a compound PA hydrogel would result in depletion of monomer and cross-linker from the second component at a rate proportional to the relative thicknesses and acrylamide/bis-acrylamide concentrations of those two components (Fig. S1A). To test this hypothesis, we added Texas red-labeled bis-acrylamide cross-linker and 100-nm green fluorescent beads to the second PA-forming solution. Fig. S1B demonstrates that bis-acrylamide leaches readily from the second PA-forming

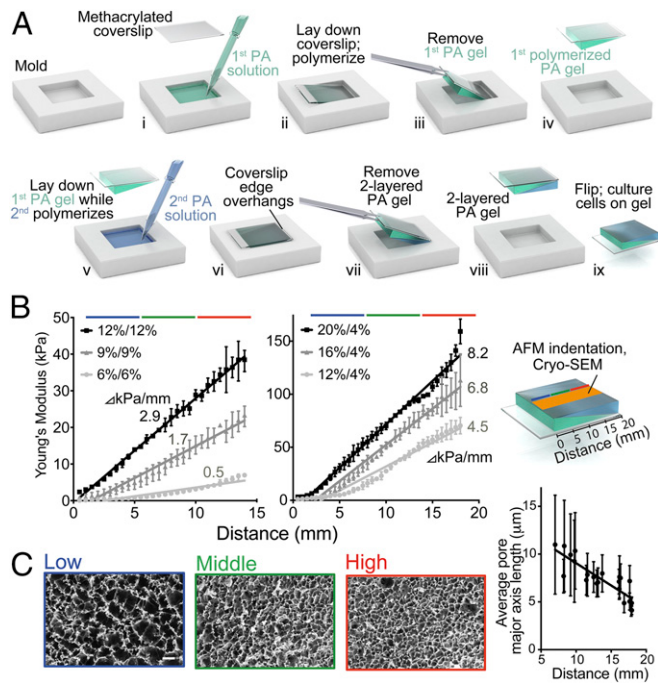


Fig. 1. Fabrication and characterization of stiffness gradient PA hydrogels. (A) A 24- × 20-mm rectangular mold is used to fabricate hydrogels in a double polymerization process creating a two-layered PA hydrogel. (B) AFM was used to probe the surface Young's modulus, E , for hydrogels composed of 12/12% = 2.9 kPa/mm ($R^2 = 0.9965$) (black squares); 9/9% = 1.7 kPa/mm ($R^2 = 0.9764$) (dark gray triangles); or 6/6% = 0.5 kPa/mm ($R^2 = 0.9041$) (light gray circles) (Left) or 20/4% = 8.2 kPa/mm ($R^2 = 0.9783$) (black squares); 16/4% = 6.8 kPa/mm ($R^2 = 0.9532$) (dark gray triangles); or 12/4% = 4.5 kPa/mm ($R^2 = 0.9415$) (light gray circles) (Right). (C, Left) Cryo-SEM images of a 12/12% PA hydrogel surface at low (blue), middle (green), and high (red) stiffness ranges. (Scale bar: 25 μm.) (Right) The corresponding graph shows pore size is inversely proportional to stiffness where the slope = $-0.4676 \mu\text{m}/\text{mm}$ ($R^2 = 0.7312$).

solution into the first PA hydrogel, but large objects (i.e., the green microbeads) do not. This result supports the idea that unpolymerized components are absorbed by the already-polymerized component, which is unsurprising given that solute diffusion through hydrogels, which has been shown to be slower than through water (39), is a feature in many drug-delivery applications (40). Furthermore, because the first component is sloped, an inherent acrylamide gradient dynamically forms within the top gel as polymerization progresses. The formation of this gradient is enhanced by the fact that as the hydrogel polymerizes, acrylamide chains lengthen and become incorporated into the cross-linked network, decreasing their diffusion coefficient and preserving the concentration gradient formed by fast diffusion into the first component. This gradient was confirmed with cryo-scanning electron microscopy (cryo-SEM) of 12/12% (vol/vol) PA hydrogels (second polymerized PA hydrogel/first polymerized PA hydrogel) at 1,000 \times and 5,000 \times magnification. Images show that the average pore size is larger in the second (top) hydrogel component although both solutions contain the same initial acrylamide:bis-acrylamide ratio (Fig. S1B). Although other systems have used polymerized PA above prepolymerized PA (17), those systems had very small diffusion distances from the surface of the gel to the underlying prepolymerized gel (~25 μm), allowing (i) an equilibrium concentration to form before polymerization occurs and (ii) the mechanical properties of the underlying stiffness layer to influence those of the upper layer.

Because the thinnest areas of the second hydrogel component suffer the greatest proportional loss of monomer/cross-linker, a

stiffness gradient subsequently results. To examine this gradient, we measured the Young's modulus of these hydrogels parallel to the ramp axis with atomic force microscopy (AFM) (41). For 20/4, 16/4, 12/4, 12/12, 9/9, and 6/6% (top gel/bottom gel, vol/vol) acrylamide solutions in which bis-acrylamide was held constant at 0.4%, linear stiffness gradients of 8.2, 6.8, 4.5, 2.9, 1.7, and 0.5 kPa/mm were observed, respectively (Fig. 1B and Table S2). Mechanical probing was repeated with a larger AFM tip to assess whether stiffness varied appreciably with probe area. Fig. S2A shows that differences in the stiffness data obtained by different AFM tip geometries are insignificant. We also used compression optical coherence elastography (OCE) (42) to characterize further any potential stiffness gradient in the *z* axis (depth), because previous studies have suggested that cells are able to feel up to 10–20 μm below the substrate surface (43, 44) when plated on very soft (~1 kPa) hydrogels. We found a maximal softening of 3.3% at a depth of 10 μm and 9.0% at a depth of 20 μm for the stiffest regions of the gradient hydrogels (Fig. S3A and Table S3). On the softest region of ~10 kPa, a depth of 20 μm shows a softening of less than 1 kPa. Although measurable, these differences are likely inconsequential for mechanosensitive responses (e.g., both 9 and 10 kPa are myogenic). This progressive softening in the *z* axis also correlates to cryo-SEM images taken of hydrogel cross-sections (Fig. S1C), which show increasing pore size with increasing distance from the culture surface.

The highest stiffness gradients measured here are mimetic of pathological stiffness gradients *in vivo* (i.e., myocardial infarction, ~7 kPa/mm) (45). Furthermore, one of the gradients (2.9 kPa/mm) spans several physiologically relevant ranges from adipose (~2 kPa) to osteoid tissue (~35 kPa) (1). As acrylamide concentration increases, e.g., 15/15% (vol/vol) acrylamide, the steepest gradients are achieved (9.8 kPa/mm), but limited monomer depletion from the second layer can compromise reproducibility (see larger error bars in Fig. S2B). For hydrogels with lower absolute acrylamide concentrations (i.e., 6/6%: 0.5 kPa/mm; 9/9%: 1.7 kPa/mm; and 12/12%: 2.9 kPa/mm), we found homogenous stiffness values perpendicular to the ramp axis, ensuring homogeneous polymerization along stiffness lines (Fig. S4).

To confirm Young's moduli gradients independently in high resolution, we used OCE (42) to capture 3D images with experimentally measured axial and lateral resolutions of 7.8 and 11 μm, respectively, up to 2–3 mm into the hydrogels (Fig. S3B). 3D reconstruction of a 12/12% (2.9 kPa/mm) PA hydrogel visualizes the stiffness gradient at the surface (Fig. S3B) as well as the ramp-angle interface between the first and second layers (Fig. S3B, Top, white line). The 5% compression required for OCE imaging resulted in a slight absolute change in reported moduli, whereas the slope of the gradient was unchanged at 2.9 kPa/mm (Fig. S3B).

The mechanism creating this stiffness gradient also suggests an accompanying pore-size gradient along the hydrogel surface, because higher degrees of crosslinking would result in smaller pore sizes in stiffer regions (38). Cryo-SEM images at 500× magnification taken at the low, middle, and high stiffness ranges on the surface of 2.9 kPa/mm PA hydrogels confirm a pore size gradient from largest (11 ± 5.2 μm) to smallest (4.1 ± 0.4 μm) from the soft to stiff ends, respectively (Fig. 1C). Stiffness-dependent behavior does not depend on pore size (38), but surface topography is known to influence cell migration (46). To exclude pore size as an influence on surface topography, 20- × 20-μm surface AFM scans corresponding to low, middle, and high stiffness ranges were generated. We found insignificant variation in surface topography between hydrogel formulations, thus excluding roughness as an influence on observed cellular behavior (Fig. S2C).

Cell-Adhesive Protein Functionalization of Gradient Hydrogels. PA hydrogels do not contain cell-adhesive domains and thus require a covalently attached protein coat such as fibronectin or collagen (8). Previous studies have confirmed that the overall amount of protein that can bind to differentially cross-linked PA does not

change as stiffness increases (36). However, concerns have been raised regarding the degree of protein tethering as a function of pore size (47), which we have shown varies across the gradient surface. To ensure that any subsequent observed differences in interaction between cells and PA hydrogels is not a result of differential levels of protein tethering, Förster resonance energy transfer (FRET) (38) was used to measure the degree of fibronectin unfolding across the gradient. ECM proteins are exposed to traction force before any subsequent ECM deformation; thus this FRET sensor is not a metric of overall traction force, which is stiffness-dependent (48, 49), but rather is a confirmation that the ECM protein itself does not experience any differential unfolding as the result of potential changes in protein–hydrogel tethering. The unfolding of the protein layer was measured as a function of the ratio of the maximum intensities of the second fluorophore (acceptor) to those of the first fluorophore (donor). FRET ratios for PA gradient hydrogels (0.5, 1.7, and 2.9 kPa/mm) in each stiffness condition (low, middle, and high) showed no significant differences (Fig. S5A). To characterize the adhesive protein layer further using a different ECM protein, collagen-coated PA hydrogels were immunostained, and pixel-intensity histograms were computed for PA hydrogels at all stiffness conditions as described in Wen et al. (38). One-way ANOVA was used to compare the area under the curve (AUC) of these histograms within each hydrogel. The 0.5, 1.7, and 2.9 kPa/mm hydrogels showed no significant differences in collagen functionalization across their surfaces ($P > 0.05$) (Fig. S5B).

Cell Migration and Durotaxis. To investigate cell migration on fibronectin-coated stiffness gradients, we used time-lapse microscopy to observe human adipose-derived stem cells (hASCs) (Fig. 2, Fig. S6, and Movies S1–S11). Durotaxis, or migration in response to a stiffness gradient, generally causes cells to migrate toward stiffer regions, with cell velocity correlating to gradient strength (19). Therefore we compared the migration of sparsely plated hASCs on a shallow gradient (2.9 kPa/mm) with the migration on a steep, pathology-mimicking gradient (8.2 kPa/mm) by calculating the instantaneous speed and direction of cells from multiple regions over 72 h (Fig. 2A). Average cell speed was similar on both gradients (Fig. 2B); however, when the cell speed was divided into components either perpendicular to or parallel to the gradient direction (*x* and *y*, respectively), the steep gradient (8.2 kPa/mm) exhibited significantly higher *y* velocities, indicating durotaxis toward the stiffer region (Fig. 2A and B). Because the average *y* velocity of cells on the 2.9-kPa/mm hydrogel was not significantly different from zero, we can conclude that the gradient did not induce biased migration. These data improve upon the durotactic threshold suggested in previous studies (17, 19) by narrowing the range in which the threshold potentially occurs to above 2.9 kPa/mm and below 8.2 kPa/mm. To rule out the possibility that cell attachment or cell proliferation is biased by the stiffness gradients, the centroid of all measured cells was calculated at low (20,000 cells per hydrogel) and high (50,000 cells per hydrogel) density cell seeding on the 2.9-kPa/mm hydrogels (depicted and quantified in Fig. 3A and B, respectively). For all samples collected after 1 d, the centroid was not significantly different from 50% in either *x* or *y*, indicating that cell attachment was not biased (Fig. 3A and B). After 6 d on the gradient hydrogels, low-density populations exhibited a slight shift toward the stiffer region (~4%). In high-density populations, this shift was much higher (~11%), suggesting that cell density plays a role in stiffness-based proliferation changes (Fig. 3A and B).

Once we established that the durotactic threshold for hASCs was above 2.9 kPa/mm, we characterized cell migration on three nondurotactic gradient gels (0.5, 1.7, and 2.9 kPa/mm). Although hASCs migrated at different speeds according to their local stiffness (i.e., cells moved faster on higher-stiffness regions), they did not exhibit any bias in the *x* or *y* direction, indicating that durotaxis was not occurring (Fig. 2C and Fig. S6). This absence of durotaxis means that cells plated on these gradient hydrogels will not preferentially move to stiffer regions, allowing the examination

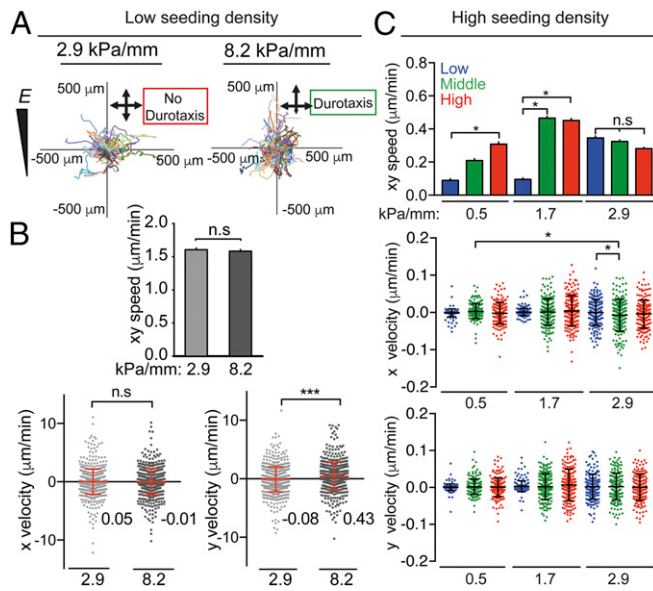


Fig. 2. Migration of hASCs on stiffness gradient hydrogels. (A) Representative hASC migration plots on 2.9-kPa/mm (Left) and 8.2-kPa/mm (Right) fibronectin-coated PA stiffness gradient hydrogels over 72 h. (B) The *xy* speed, *x* velocity, and *y* velocity (in micrometers per minute) on 2.9- and 8.2-kPa/mm fibronectin-coated PA gels on which the positive *y* velocity vector is toward the stiffer end of the hydrogel. (C) Average speed (*xy*) and *x* and *y* velocity over 72 h of hASCs on low (blue), middle (green), and high (red) stiffness ranges of 0.5-, 1.7-, and 2.9-kPa/mm gradient hydrogels. Cells were seeded at low density (<20,000 cells per well) for A and B and at high density (>50,000 cells per well) for C. For A and B, all data are shown as mean \pm SEM (speed) and mean \pm SD (velocity) (>695 cells analyzed). For C, $n = 6$ (30 cells tracked per n). In stiffness runs along the *y* axis, more positive = stiffer. Blue = low, green = middle, and red = high stiffness range. For all: * $P < 0.05$, *** $P < 0.001$; n.s., not significant.

of cell behavior and protein expression in response to a continuous range of stiffnesses without the confounding effect of biased migration.

Stem Cell Mechanotransduction and Differentiation. In this set-up, gradients can be fabricated both above and below the durotactic threshold, giving this system dual utility. As explored above, gels with gradients above the durotactic-promoting threshold can be used to analyze cell migration toward stiffer or softer regions. Perhaps more interestingly, gels with gradients below the durotactic threshold can be used as single-well platforms for analyzing cellular responses to a wide range of static substrate stiffnesses without the confounding effect of biased cell migration. We used the inability of the 2.9-kPa/mm gradients to induce durotaxis (Fig. 2C and Fig. S6) to our advantage to investigate mechanotransduction and differentiation decoupled from durotaxis.

To demonstrate the ability to assess cellular morphological characteristics in a high content fashion, nuclei and the actin cytoskeleton were stained on these gradient hydrogels, allowing the analysis of thousands of cells in a single well (Fig. 3A). We found that in hASCs, both the cell-spread area and the nuclear area increase with stiffness (Fig. 3D). In addition, despite steady increases in cross-sectional area, the aspect ratio of both cells and nuclei remained consistent across the entire stiffness range, suggesting that the stresses contributing to nuclear expansion were isotropic (Fig. 3C). This finding is in contrast to data obtained from C2C12 mouse myoblasts, in which the cellular-spread area increased with stiffness but the nuclear cross-sectional area remained generally constant (Fig. 3D). Because nuclear stiffness has been shown to increase as differentiation progresses, it follows that nuclei in more terminally differentiated cells would compress less in response to traction forces (50). Thus, this system

presents an opportunity for high content analysis of simple morphological responses of different cell types. This system can also be extended to specialized cell populations (i.e., knockouts) in which interesting morphological changes (cell aspect ratio, focal adhesion area, and so forth) in response to substrate stiffness can be assessed.

The use of immunofluorescence allows the examination of stiffness-dependent cell behavior beyond morphological characterization. The nuclear intermediate filament Lamin A exhibits scaled expression with tissue stiffness (51) and a dose-dependent mechanosensing response. To determine to what extent switch-like vs. dose-dependent signaling regulates behavior at intermediate stiffness in single cells, hASCs were stained for Lamin A and Lamin B on 2.9-kPa/mm-gradient hydrogels (Fig. 4A). Lamin A expression was found to scale in a logarithmic dose-dependent manner in response to stiffness (Fig. 4B), i.e., exhibiting quick increases in intensity between 2 and 18 kPa and marginally slower increases above 18 kPa. These high stiffness-resolution data are consistent with previous reports of logarithmic increases of Lamin A expression in single cells that assayed only three distinct stiffness values (51). Furthermore, by staining the same cell populations for Lamin A and Lamin B, we obtained individual Lamin A/Lamin B ratios for thousands of cells over a range of physiological stiffnesses, revealing an exponential increase in this ratio as stiffness increases (Fig. 4G). In contrast with hASCs, C2C12 cells showed less stiffness-dependent Lamin A expression, with nuclear Lamin A levels saturating above 10 kPa (Fig. 4I). Again, this finding

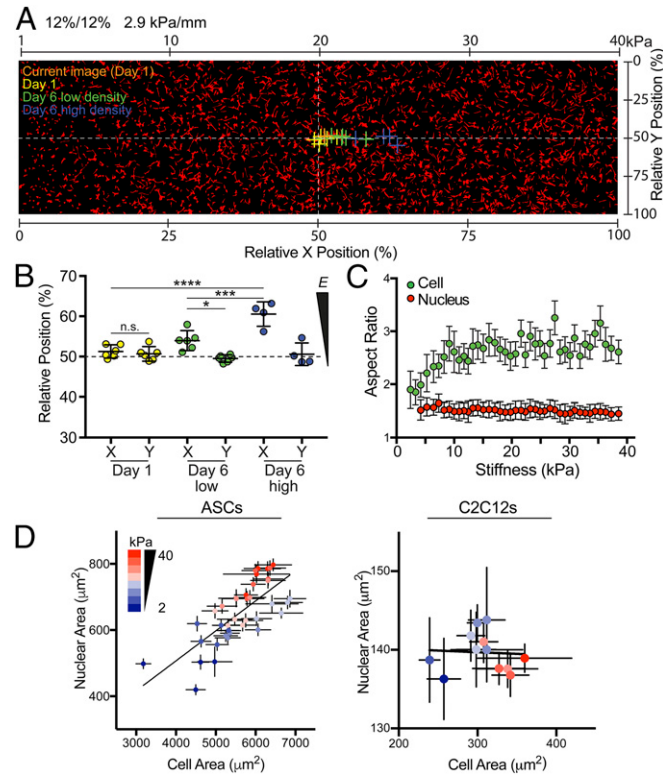


Fig. 3. Centroid and morphological characteristics of hASCs and C2C12s on stiffness gradient hydrogels. (A) Centroids of cell on gradient gels are indicated with a cross for current image at day 1 (orange), day 1 (yellow), day 6 at low density (green), and day 6 at high density (blue). White dashed lines intersect at the center of the image (relative *x* and *y* positions of 50%). (B) Relative *x* and *y* positions from A are graphed. (C) Cellular (green) and nuclear (red) aspect ratios are plotted as a function of Young's modulus, *E*. (D) Nuclear area (in square millimeters) vs. cell area (in square millimeters) for hASCs (Left) and C2C12s (Right) as a function of stiffness (2 kPa: blue to 40 kPa: red). * $P < 0.05$, *** $P < 0.001$, **** $P < 0.0001$, n.s., not significant.

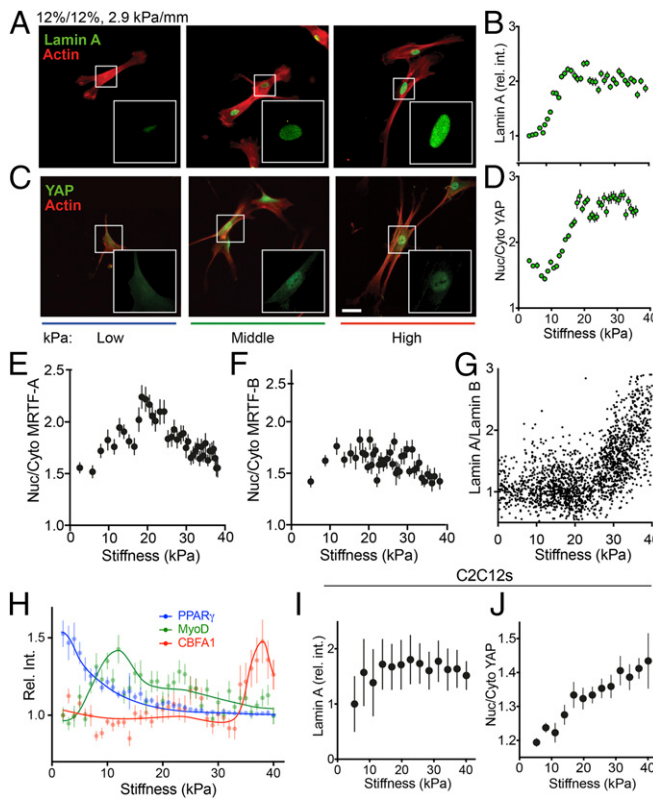


Fig. 4. Mechanotransduction and differentiation of hASCs on stiffness gradient hydrogels. (A) Representative images of hASCs plated on fibronectin-coated stiffness gradient hydrogels stained for Lamin A (green) and actin (red) for low (blue), middle (green), and high (red) stiffness regions of the hydrogel. (B) Lamin A relative intensity (rel. int.) plotted vs. stiffness. (C) Representative images for YAP (green) and actin (red) as in A. (D) Nuclear-to-cytoplasmic ratio (Nuc/Cyto) of YAP. (E and F) Nuclear-to-cytoplasmic ratio of MRTF-A (E) and MRTF-B (F) plotted as a function of stiffness. (G) The ratio of Lamin A to Lamin B is plotted vs. stiffness. (H) Expression of differentiation markers (rel. int.) of PPAR γ (blue), MyoD (green), and CBFA1 (red) vs. stiffness. (I and J) C2C12 cells were examined for Lamin A expression (rel. int.) (I) and nuclear to cytoplasmic ratio of YAP (J) as a function of stiffness. (Scale bar: 50 μ m; scale in A is identical to C.)

mirrors previous observations that more terminally differentiated cells tend to have more stable patterns of Lamin A expression (52).

YAP displays a biphasic regulation pattern by alternatively localizing to the cytoplasm on soft matrices and to the nucleus on stiff matrices (53). This substrate stiffness-dependent behavior was recently analyzed in more detail, increasing the stiffness resolution to six discrete static PA hydrogels, allowing discernment of the specific stiffness regime in which YAP translocates to the nucleus (49). However, these and other studies have struggled to identify the stiffness range that shows a transition-level translocation, as opposed to on/off behavior. On 2.9-kPa/mm gradient hydrogels, the nucleus/cytoplasm ratio of YAP appeared sigmoidal, with a minimum ratio found from 2–12 kPa, followed by a linear increase in nuclear localization from 12–20 kPa and a saturated nuclear localization state above 20 kPa (Fig. 4 C and D). This result suggests that the nuclear translocation of YAP is indeed stiffness-dose dependent for certain stiffness ranges, with a fairly broad sigmoidal transition zone that includes physiological stiffness values, in contrast to prior suggestions of binary, switch-like localization patterns. Finding transition zones like these can have important implications in the understanding of many signaling pathways, because they indicate that intermediate levels of expression or localization potentially could result in outcomes different from “on” or “off.” Indeed, C2C12 myoblasts, which have been shown to have a pattern of YAP expression and

nuclear localization different from that of stem cells, were found to have a much broader transition zone, with nuclear localization increasing steadily from 2 to 38 kPa (Fig. 4J) (54).

The transcription factors MRTF-A and MRTF-B, also known as “Mkl1/MAL” and “Mkl2/MAL16,” have been shown to shuttle naturally between the cytoplasm and the nucleus (55), to play a role in myogenic differentiation (56), and to be directly affected by the actin polymerization state of the cell (57). MRTF-A interactions with YAP have generated substantial interest in the nuclear localization patterns of MRTF-A (58–60), but to date nearly all investigations that test stiffness variations have analyzed only two distinct values (61, 62). Leveraging our gradient system, we analyzed expression patterns of MRTF-A and MRTF-B in hASCs plated for 24 h on 2.9-kPa/mm hydrogels and found that although MRTF-B localization was independent of stiffness (Fig. 4F), MRTF-A expression peaked at ~20 kPa (Fig. 4E). This finding is in contrast with reported time-dependent increases in nuclear localization of MRTF-A in hMSCs on 100-kPa PA substrates (62), although we did not analyze supraphysiological stiffnesses higher than 40 kPa. However, these results are intriguing in that MRTF-A has been shown to regulate miRNAs with roles in myogenic differentiation, a process that occurs near the stiffness region at which we observed MRTF-A to peak in ref. 63.

To explore this platform’s utility further, specifically in the context of stem cells, we analyzed stiffness-dependent hASC differentiation after 6 d on 2.9-kPa/mm gradient hydrogels. In agreement with previous studies (1), the expression of the adipogenic marker PPAR γ was found to peak at low stiffnesses ($E < 3$ kPa) and to decrease quickly as stiffness increased (Fig. 4H, blue). Similarly, expression of the myogenic transcription factor MyoD was found to peak at $E \sim 12$ kPa (Fig. 4H, green), and CBFA1, an osteogenic marker, was highest around $E \sim 36$ kPa (Fig. 4H, red), also in agreement with a large body of literature on mechanosensitive myogenic and osteogenic differentiation.

Conclusion

Nearly all phenomena in cell biology are affected to some degree by substrate stiffness, from stem cell differentiation (1) to cancer cell chemoresistance (64) to heart cell function (65). The stiffness gradient platform described here allows the investigator to test a wide range of mechanical induction signals on the same surface. Furthermore, because the slope of stiffness built into this technology is easily tunable, it can be customized to a wide variety of biological conditions or disease processes under investigation; shallow slopes can isolate stiffness as an inductive factor, and steeper slopes can elicit durotaxis. This method offers a simpler solution than those previously available to fabricate synthetic stiffness gradients and is easily reproducible because it requires only a few simple components that can be procured and assembled in any biochemistry laboratory. Most importantly, the shallower gradients created by this method enable observations of more subtle behaviors in stem cells, e.g., the dose-dependent rather than switch-like responses of YAP to intermediate stiffness values, exemplifying the utility of these gradient hydrogels.

Materials and Methods

PA gradient hydrogels were fabricated using a two-layer polymerization method. After characterization of hydrogels, human ASCs or C2C12 cells were cultured on fibronectin-functionalized hydrogels. Time-lapse microscopy was used to study cell migration, and immunocytochemistry was used to measure cell distribution and to show cell mechanotransduction and stem cell differentiation. Further details about mold fabrication, cell assays, and statistical analyses can be found in *SI Materials and Methods*.

The use of freshly aspirated human adipose tissue was approved by the University of California, San Diego human research protections program (Project # 101878).

ACKNOWLEDGMENTS. We thank Christine Mollenhauer for fibronectin purification, Ayla Sessions for atomic force microscopy, Luke Major for immunostaining, and Dr. Günter Majer for fruitful discussions on diffusion. This work was supported by a Sydney Medical School Dean’s Award (to W.J.H.), Max Planck Institute Postdoctoral Fellowships (to J.L.Y. and

A.W.H.), European Research Council Grant 294852 SynAd (to J.P.S.), the Federal Ministry of Education and Research of Germany and the Max Planck Society (J.P.S.), the excellence cluster CellNetworks at the University of Heidelberg (J.P.S.), National Science Foundation Graduate Research Fellowships (to H.T.-W. and J.H.W.), National Institutes of Health Grants DP2OD006460 and R01AG045428 (to A.J.E.), Australian Research Council

Grant DP160104662 (to B.-N.V.), the University of Western Australia William and the Marlene Schrader Fund (P.W.), Australian Research Council Grant DP140104443 (to D.D.S.), National Health and Medical Research Council Grant PG1098449 (to Y.S.C.), and Heart Research Australia Grant 2014-07 (to Y.S.C.). J.P.S. is the Weston Visiting Professor at the Weizmann Institute of Science.

1. Engler AJ, Sen S, Sweeney HL, Discher DE (2006) Matrix elasticity directs stem cell lineage specification. *Cell* 126:677–689.
2. Fu J, et al. (2010) Mechanical regulation of cell function with geometrically modulated elastomeric substrates. *Nat Methods* 7:733–736.
3. Yang MT, Fu J, Wang YK, Desai RA, Chen CS (2011) Assaying stem cell mechanobiology on microfabricated elastomeric substrates with geometrically modulated rigidity. *Nat Protoc* 6:187–213.
4. Li Jeon N, et al. (2002) Neutrophil chemotaxis in linear and complex gradients of interleukin-8 formed in a microfabricated device. *Nat Biotechnol* 20:826–830.
5. Liu X, et al. (2015) Surface chemical gradient affects the differentiation of human adipose-derived stem cells via ERK1/2 signaling pathway. *ACS Appl Mater Interfaces* 7:18473–18482.
6. Pettit EJ, Fay FS (1998) Cytosolic free calcium and the cytoskeleton in the control of leukocyte chemotaxis. *Physiol Rev* 78:949–967.
7. Engler AJ, et al. (2004) Substrate compliance versus ligand density in cell on gel responses. *Biophys J* 86:617–628.
8. Pelham RJ, Wang YL (1998) Cell locomotion and focal adhesions are regulated by the mechanical properties of the substrate. *Biol Bull* 194:348–9, discussion 349–50.
9. Lo C-M, Wang H-B, Dembo M, Wang Y-L (2000) Cell movement is guided by the rigidity of the substrate. *Biophys J* 79:144–152.
10. Wang P-Y, Tsai W-B, Voelcker NH (2012) Screening of rat mesenchymal stem cell behaviour on polydimethylsiloxane stiffness gradients. *Acta Biomater* 8:519–530.
11. Deroanne CF, Lapierre CM, Nusgens BV (2001) In vitro tubulogenesis of endothelial cells by relaxation of the coupling extracellular matrix-cytoskeleton. *Cardiovasc Res* 49:647–658.
12. Flanagan LA, Rebaza LM, Derzic S, Schwartz PH, Monuki ES (2006) Regulation of human neural precursor cells by laminin and integrins. *J Neurosci Res* 83:845–856.
13. Choi YS, Vincent LG, Lee AR, Dobke MK, Engler AJ (2012) Mechanical derivation of functional myotubes from adipose-derived stem cells. *Biomaterials* 33:2482–2491.
14. Holle AW, et al. (2016) High content image analysis of focal adhesion-dependent mechanosensitive stem cell differentiation. *Integr Biol* 8:1049–1058.
15. Discher DE, Janmey P, Wang Y-L (2005) Tissue cells feel and respond to the stiffness of their substrate. *Science* 310:1139–1143.
16. Engler AJ, et al. (2004) Myotubes differentiate optimally on substrates with tissue-like stiffness: Pathological implications for soft or stiff microenvironments. *J Cell Biol* 166:877–887.
17. Choi YS, et al. (2012) The alignment and fusion assembly of adipose-derived stem cells on mechanically patterned matrices. *Biomaterials* 33:6943–6951.
18. Tse JR, Engler AJ (2011) Stiffness gradients mimicking in vivo tissue variation regulate mesenchymal stem cell fate. *PLoS One* 6:e15978.
19. Vincent LG, Choi YS, Alonso-Latorre B, del Álamo JC, Engler AJ (2013) Mesenchymal stem cell durotaxis depends on substrate stiffness gradient strength. *Biotechnol J* 8:472–484.
20. Flanagan LA, Ju Y-E, Marg B, Osterfield M, Janmey PA (2002) Neurite branching on deformable substrates. *Neuroreport* 13:2411–2415.
21. Solon J, Levental I, Sengupta K, Georges PC, Janmey PA (2007) Fibroblast adaptation and stiffness matching to soft elastic substrates. *Biophys J* 93:4453–4461.
22. Paszek MJ, et al. (2005) Tensional homeostasis and the malignant phenotype. *Cancer Cell* 8:241–254.
23. Wang H-B, Dembo M, Wang Y-L (2000) Substrate flexibility regulates growth and apoptosis of normal but not transformed cells. *Am J Physiol Cell Physiol* 279:C1345–C1350.
24. Welch DR, et al. (2000) Transfection of constitutively active mitogen-activated protein/extracellular signal-regulated kinase kinase confers tumorigenic and metastatic potentials to NIH3T3 cells. *Cancer Res* 60:1552–1556.
25. Kim TH, et al. (2015) Creating stiffness gradient polyvinyl alcohol hydrogel using a simple gradual freezing-thawing method to investigate stem cell differentiation behaviors. *Biomaterials* 40:51–60.
26. Hopp I, et al. (2013) The influence of substrate stiffness gradients on primary human dermal fibroblasts. *Biomaterials* 34:5070–5077.
27. Kuo CHR, Xian J, Brenton JD, Franzke K, Sivaniah E (2012) Complex stiffness gradient substrates for studying mechanotactic cell migration. *Adv Mater* 24:6059–6064.
28. Nemir S, Hayenga HN, West JL (2010) PEGDA hydrogels with patterned elasticity: Novel tools for the study of cell response to substrate rigidity. *Biotechnol Bioeng* 105:636–644.
29. Tse JR, Engler AJ (2010) Preparation of hydrogel substrates with tunable mechanical properties. *Curr Protoc Cell Biol* 10.16.1–10.16.16.
30. Wong JY, Velasco A, Rajagopalan P, Pham Q (2003) Directed movement of vascular smooth muscle cells on gradient-compliant hydrogels. *Langmuir* 19:1908–1913.
31. Johnson PM, Reynolds TB, Stansbury JW, Bowman CN (2005) High throughput kinetic analysis of photopolymer conversion using composition and exposure time gradients. *Polymer (Guildf)* 46:3300–3306.
32. Marklein RA, Burdick JA (2010) Spatially controlled hydrogel mechanics to modulate stem cell interactions. *Soft Matter* 6:136–143.
33. Sunyer R, Jin AJ, Nossal R, Sackett DL (2012) Fabrication of hydrogels with steep stiffness gradients for studying cell mechanical response. *PLoS One* 7:e46107.
34. Hartman CD, Isenberg BC, Chua SG, Wong JY (2016) Vascular smooth muscle cell durotaxis depends on extracellular matrix composition. *Proc Natl Acad Sci USA* 113:11190–11195.
35. Brandl F, Sommer F, Goepferich A (2007) Rational design of hydrogels for tissue engineering: Impact of physical factors on cell behavior. *Biomaterials* 28:134–146.
36. Isenberg BC, Dimilla PA, Walker M, Kim S, Wong JY (2009) Vascular smooth muscle cell durotaxis depends on substrate stiffness gradient strength. *Biophys J* 97:1313–1322.
37. Chao P-HG, Sheng S-C, Chang W-R (2014) Micro-composite substrates for the study of cell-matrix mechanical interactions. *J Mech Behav Biomed Mater* 38:232–241.
38. Wen JH, et al. (2014) Interplay of matrix stiffness and protein tethering in stem cell differentiation. *Nat Mater* 13:979–987.
39. White ML, Dorion GH (1961) Diffusion in a crosslinked acrylamide polymer gel. *J Polym Sci A Polym Chem* 55:731–740.
40. Hoare TR, Kohane DS (2008) Hydrogels in drug delivery: Progress and challenges. *Polymer (Guildf)* 49:1993–2007.
41. Kaushik G, Fuhrmann A, Cammarato A, Engler AJ (2011) In situ mechanical analysis of myofibrillar perturbation and aging on soft, bilayered *Drosophila* myocardium. *Biophys J* 101:2629–2637.
42. Kennedy KM, et al. (2015) Quantitative micro-elastography: Imaging of tissue elasticity using compression optical coherence elastography. *Sci Rep* 5:15538.
43. Buxboim A, Rajagopal K, Brown AEX, Discher DE (2010) How deeply cells feel: Methods for thin gels. *J Phys Condens Matter* 22:194116.
44. Sen S, Engler AJ, Discher DE (2009) Matrix strains induced by cells: Computing how far cells can feel. *Cell Mol Bioeng* 2:39–48.
45. Berry MF, et al. (2006) Mesenchymal stem cell injection after myocardial infarction improves myocardial compliance. *Am J Physiol Heart Circ Physiol* 290:H2196–H2203.
46. Sun Y, Jallerat Q, Szymanski JM, Feinberg AW (2015) Conformal nanopatterning of extracellular matrix proteins onto topographically complex surfaces. *Nat Methods* 12:134–136.
47. Trappmann B, et al. (2012) Extracellular-matrix tethering regulates stem-cell fate. *Nat Mater* 11:642–649.
48. Califano JP, Reinhart-King CA (2010) Substrate stiffness and cell area predict cellular traction stresses in single cells and cells in contact. *Cell Mol Bioeng* 3:68–75.
49. Elosgui-Artola A, et al. (2016) Mechanical regulation of a molecular clutch defines force transmission and transduction in response to matrix rigidity. *Nat Cell Biol* 18:540–548.
50. Pajerowski JD, Dahl KN, Zhong FL, Sammak PJ, Discher DE (2007) Physical plasticity of the nucleus in stem cell differentiation. *Proc Natl Acad Sci USA* 104:15619–15624.
51. Swift J, et al. (2013) Nuclear lamin-A scales with tissue stiffness and enhances matrix-directed differentiation. *Science* 341:1240104.
52. Constantinescu D, Gray HL, Sammak PJ, Schatten GP, Csoka AB (2006) Lamin A/C expression is a marker of mouse and human embryonic stem cell differentiation. *Stem Cells* 24:177–185.
53. Dupont S, et al. (2011) Role of YAP/TAZ in mechanotransduction. *Nature* 474:179–183.
54. Watt KI, et al. (2010) Yap is a novel regulator of C2C12 myogenesis. *Biochem Biophys Res Commun* 393:619–624.
55. Vartiainen MK, Guettler S, Larijani B, Treisman R (2007) Nuclear actin regulates dynamic subcellular localization and activity of the SRF cofactor MAL. *Science* 316:1749–1752.
56. Selvaraj A, Prywes R (2003) Megakaryoblastic leukemia-1/2, a transcriptional co-activator of serum response factor, is required for skeletal myogenic differentiation. *J Biol Chem* 278:41977–41987.
57. Miralles F, Posern G, Zaromytidou A-I, Treisman R (2003) Actin dynamics control SRF activity by regulation of its coactivator MAL. *Cell* 113:329–342.
58. Speight P, Kofler M, Szászi K, Kapus A (2016) Context-dependent switch in chemo/mechanotransduction via multilevel crosstalk among cytoskeleton-regulated MRTF and TAZ and TGFβ-regulated Smad3. *Nat Commun* 7:11642.
59. Yu OM, Miyamoto S, Brown JH (2015) Myocardin-related transcription factor A and Yes-associated protein exert dual control in G protein-coupled receptor- and RhoA-mediated transcriptional regulation and cell proliferation. *Mol Cell Biol* 36:39–49.
60. Kim T, et al. (2017) MRTF potentiates TEAD-YAP transcriptional activity causing metastasis. *EMBO J* 36:520–535.
61. Shiwen X, et al. (2015) A role of myocardin related transcription factor-A (MRTF-A) in scleroderma related fibrosis. *PLoS One* 10:e0126015.
62. Li CX, et al. (2017) MicroRNA-21 preserves the fibrotic mechanical memory of mesenchymal stem cells. *Nat Mater* 16:379–389.
63. Xin M, et al. (2009) MicroRNAs miR-143 and miR-145 modulate cytoskeletal dynamics and responsiveness of smooth muscle cells to injury. *Genes Dev* 23:2166–2178.
64. Holle AW, Young JL, Spatz JP (2016) In vitro cancer cell-ECM interactions inform in vivo cancer treatment. *Adv Drug Deliv Rev* 97:270–279.
65. Young JL, Engler AJ (2011) Hydrogels with time-dependent material properties enhance cardiomyocyte differentiation in vitro. *Biomaterials* 32:1002–1009.
66. Smal I, Loog M, Niessen W, Meijering E (2010) Quantitative comparison of spot detection methods in fluorescence microscopy. *IEEE Trans Med Imaging* 29:282–301.
67. Vo B-N, Vo B-T, Phung D (2014) Labeled random finite sets and the Bayes multi-target tracking filter. *IEEE Trans Signal Process* 62:6554–6567.
68. Kamentky L, et al. (2011) Improved structure, function and compatibility for CellProfiler: Modular high-throughput image analysis software. *Bioinformatics* 27:1179–1180.